# Effect of Weld Pool Deformation on Weld Penetration in Stationary Gas Tungsten Arc Welding

*The influence of four distinct driving forces in weld pool convection are evaluated in developing a model*

BY S. -D. KIM AND S. -J. NA

ABSTRACT. The effect of weld pool surface deformation on weld joint penetration under the arc pressure has been studied in stationary gas tungsten arc welding (GTAW), by considering the four driving forces for weld pool convection: electromagnetic force, buoyancy force, aerodynamic drag force, and surface tension force at the weld pool surface. In the numerical simulation, difficulties associated with the irregular shape of the deformed weld pool surface and the moving liquid-solid interface have been successfully overcome by adopting a boundary-fitted coordinate system, which eliminates the analytical complexity there. This method also has the capacity to handle the time-dependent changing solution domain of the moving boundary problem and could be applied effectively to this transient weld pool development problem with the phase change condition and moving boundary, such as at the deformed weld pool surface and the liquid-solid interface.

## Introduction

When current flows through a conductor, it generates a circumferential magnetic field. The interaction between the current and this self-induced magnetic field produces a body force, called the Lorentz force, which is toward the central axis of the magnetic field loop. The constricting Lorentz force is balanced by the radial pressure gradient in the arc acting in the opposite direction. If the arc has a divergent current distribution, the current density near the tungsten electrode will be higher than the current density near the base metal. Thus, the static gas pressure at the cathode end is higher than that at the anode end. The difference of static gas pressure between anode and cathode will produce a plasma jet toward the anode in the gas tungsten arc welding (GTAW) process. The stagnation pressure generated when the plasma jet is arrested on the anode surface is called the arc pressure.

In GTAW, arc pressure is caused by the momentum transfer of the impinging plasma jet on the weld pool and has been thought by many to be a major factor in producing the surface deformation of the weld pool and weld defects such as humped beads, finger penetration and undercutting. When a plasma jet impinges on the surface of a liquid, it may induce flow motion in the liquid. Thus, arc pressure also influences the weld penetration and the shape of the liquid-solid interface due to the induced liquid motion in the weld pool. Shaw has pointed out that turbulence in the welding arc plasma may have a gross effect on the resulting weld geometry (Ref. 1). Friedman has shown that the pressure of the jet may depress the molten weld pool and hence affect the weld penetration and heat transfer (Ref. 2).

In general, the weld pool convection is driven by four distinct forces: buoyancy force, electromagnetic force, surface tension force and aerodynamic drag force (to be expressed as the drag force) (Ref. 3). Up to the present, a number of researchers have considered only three forces, excluding the drag force, as driving forces for weld pool convection (Refs. 3, 4). But in the present study, the drag force and the arc pressure exerted by the impinging plasma jet, were also considered. Accordingly, the general assumption that the weld pool surface is flat could be eliminated in the present study.

The fact that the weld pool size increases and changes its shape with time poses a moving boundary problem, in which the solution of the liquid-solid interface is not known *a priori*, but is a part of the overall solution (Ref. 5). For treatment of such a problem in the context of discrete numerical methods, most previous studies have used a method which employs a grid system that is fixed in space and time and in which the phase boundary traverses the mesh system during the evolution process (Ref. 6). A weak point of this method is the treatment of boundary conditions at the moving interface and the weld pool surface (Ref. 7). For example, in the consideration of latent heat at the moving interface where the phase changes, the onset of the phase change at any node is indicated when the temperature at the two successive time increments straddles the phase transition temperature (Ref. 8). When the onset of melting is detected, the node temperature is set equal to the melting temperature, and the energy input to the node from neighboring nodes is accumulated into an internal energy variable. The node temperature is not permitted to exceed the transition value until the accumulated energy is equal to the latent heat of the material in the node. As a result, this method requires the use of very fine grids, which in turn increase the computing time, and further, a fine spatial grid restricts the size of the maximum time step. The major difficulty inherent in this method is, however, associated with the irregular boundaries which require interpolation between boundaries and interior node points. Such

**KEY WORDS**

Weld Pool
Surface Deformation
Weld Penetration
Computer Modeling
GTAW
Weld Current
Heat Transfer
Flow Pattern
Electromagnetic Force
Surface Tension

*S. -D. KIM is with the Research Institute of Hyundai Precision and Industrial Co., Ltd., Seoul, Korea. S. -J. NA is an Associate Professor, Department of Production Engineering, Korea Advanced Institute of Science and Technology, Seoul, Korea.*

interpolation between node points to represent the boundary conditions on a curved boundary passing through a rectangular coordinate grid may lead to a poor application of the boundary conditions. Therefore, if a boundary-fitted coordinate system, maintaining the liquid-solid interface and the weld pool surface coincident with a particular coordinate line, can be used, the implementation of the latent heat effect and the formulation of boundary conditions is easy and straightforward, and the finite difference approach can give a very smooth solution that retains the continuity of derivatives (Ref. 9).

To handle the irregularly shaped liquid-solid interface and weld pool surface, a numerical mapping technique was chosen in this study, which generates a boundary-fitted coordinate system and offers some possibilities in the spacing and structure of the grid system. That is, by transforming the moving physical grid system, which is, in general, nonorthogonal, onto a rectangular and uniformly spaced computational domain, which is fixed in time and space, irregular boundaries of the physical grid system could be easily treated.

## Formulation

### Governing Equation

In order to develop the mathematical model, the process was physically defined as a spatially distributed heat and current flux falling on the free surface, inducing the conductive and convective heat transfer. The following additional assumptions have been adopted for further simplification:

1) The flow is Newtonian and incompressible.

2) The flow is laminar and axially symmetrical.

3) Physical properties are constant except for the thermal conductivity, the specific heat and the density in the buoyancy term (Boussinesq approximation).

4) Heat and current distribution has Gaussian characteristics.

Then the governing equations, describing the continuity equation, the momentum equation and the energy equation for unsteady heat and mass transfer in the liquid and solid region, may be written in axisymmetric cylindrical coordinates as follows (Ref. 10):

$$\frac{1}{r}\frac{\partial}{\partial r}(\rho r v_r) + \frac{\partial}{\partial z}(\rho v_z) = 0 \qquad (1)$$

$$\rho\frac{Dv_r}{Dt} = -\frac{\partial p}{\partial r} + \mu\left(\nabla^2 v_r - \frac{v_r}{r^2}\right) + F_r \qquad (2)$$

$$\rho\frac{Dv_z}{Dt} = -\frac{\partial p}{\partial z} + \mu\nabla^2 v_z + F_z \qquad (3)$$

$$\frac{DT}{Dt} = \bar{\alpha}\nabla^2 T \qquad (4)$$

where $\bar{\alpha} = \begin{cases} \bar{\alpha}_\ell \text{ in molten state} \\ \bar{\alpha}_s \text{ in solid state} \end{cases}$

and $v_r$, $v_z$ mean r- and z-component of liquid metal velocity vector V, respectively.

In arc welding, there are four distinct driving forces for weld pool convection: buoyancy force, electromagnetic force, drag force, and surface tension force at the weld pool surface. The temperature difference in the weld pool gives rise to a buoyancy force and the passage of the current through the weld pool creates an electromagnetic force field. The other driving forces for convection, the drag force and the surface tension force, are treated as boundary conditions, as will be shown later. Therefore, in Equations 2 and 3 the body force term can be expressed as follows:

$$F_r = -B_\theta \cdot J_z \qquad (5A)$$

$$F_z = B_\theta \cdot J_r - \rho\bar{\beta}g(T - T_\ell) \qquad (5B)$$

where $J_r = \frac{I}{2\pi}\int_0^\infty \lambda J_1(\lambda r) \cdot \text{EXP}(-\lambda^2 r_i^2/12) \cdot \frac{\cosh\lambda(H-z)}{\sinh(\lambda H)}\,d\lambda$,

$J_z = \frac{I}{2\pi}\int_0^\infty \lambda J_0(\lambda r) \cdot \text{EXP}(-\lambda^2 r_i^2/12) \cdot \frac{\sinh\lambda(H-z)}{\sinh(\lambda H)}\,d\lambda$,

$B_\theta = \frac{\mu_m I}{2\pi}\int_0^\infty J_1(\lambda r) \cdot \text{EXP}(-\lambda^2 r_i^2/12) \cdot \frac{\sinh\lambda(H-z)}{\sinh(\lambda H)}\,d\lambda$,

$J_r$, $J_z$ mean the r- and z-component of the current density vector J, and $B_\theta$ is the $\theta$-component of the magnetic flux vector B.

In the present problem, it is convenient to write these in the vorticity-stream function form rather than the primitive form. The Navier-Stokes equations in the primitive variables demand the specification of boundary conditions on pressure. But this is difficult to specify in this problem and hence the following vorticity-stream function form of these equations is generally preferred:

$$\omega = \frac{\partial v_r}{\partial z} - \frac{\partial v_z}{\partial r} \qquad (6A)$$

$$v_r = -\frac{1}{r}\frac{\partial\psi}{\partial z} \qquad (6B)$$

$$v_z = \frac{1}{r}\frac{\partial\psi}{\partial r} \qquad (6C)$$

$$\rho\frac{\partial\omega}{\partial t} + \frac{\partial}{\partial r}(\rho v_r\omega) + \frac{\partial}{\partial z}(\rho v_z\omega) = \mu\left(\frac{\partial^2\omega}{\partial r^2} + \frac{1}{r}\frac{\partial\omega}{\partial r} + \frac{\partial^2\omega}{\partial z^2} - \frac{\omega}{r^2}\right) + \rho\bar{\beta}g\frac{\partial}{\partial r}(T - T_\ell) - \left\{\frac{\partial}{\partial r}\left(B_\theta J_r\right) + \frac{\partial}{\partial z}\left(B_\theta J_z\right)\right\} \qquad (7)$$

$$-\frac{1}{r}\left(\frac{\partial^2\psi}{\partial r^2} - \frac{1}{r}\frac{\partial\psi}{\partial r} + \frac{\partial^2\psi}{\partial z^2}\right) = \omega \qquad (8)$$

where $\omega$ and $\psi$ mean the vorticity and the stream function, respectively.

### Boundary Condition

To complete the mathematical description of the problem, the boundary conditions are shown in Fig. 1 and specified as follows:

$$\Gamma_{\ell_1}: \nabla T \cdot \vec{n}\xi = 0 \quad , v_r = 0$$

$$\Gamma_{\ell_2}: \nabla T \cdot \vec{n}\eta = -q_\alpha/k^*$$

$$\Gamma_{\ell_3}: \nabla T \cdot \vec{n}\xi = q_\alpha/k^*$$

$$\Gamma_{\ell_4}: T = T_\ell \quad , v_r = v_z = 0 \qquad (9)$$

$$\Gamma_{s_1}: \begin{cases} \nabla T \cdot \vec{n}\xi = 0 & (r = 0) \\ \nabla T \cdot \vec{n}\xi = -q_c/k^* & (r \neq 0) \end{cases}$$

$$\Gamma_{s_2}: T = T_\ell$$

$$\Gamma_{s_3}: \nabla T \cdot \vec{n}\xi = q_\alpha/k^*$$

$$\Gamma_{s_4}: \nabla T \cdot \vec{n}\eta = -q_c/k^*$$

where $k^* = \begin{cases} k_\ell \text{ in molten state} \\ k_s \text{ in solid state} \end{cases}$

$q_\alpha$ means the heat density distribution of the arc $\left(= \frac{3Q}{\pi r_q^2}\text{EXP}\left\{-3\left(\frac{r}{r_q}\right)^2\right\}\right)$ and $q_c$ means the heat loss by free convection $(= h(T - T_\infty))$.

At the free surface ($\Gamma_{\ell_2}$ and $\Gamma_{\ell_3}$), the balance between the shear stress and the sum of the drag force caused by the radially outward surface flow of the impinging plasma jet and the surface tension force caused by the temperature gradient, requires the boundary condition to be written as follows:

$$\omega = \frac{\partial v_r}{\partial z} - \frac{\partial v_z}{\partial r} = -\frac{1}{\mu}\left\{\left(\frac{d\sigma}{dT}\right)\left(\frac{\partial T}{\partial\ell}\right)(\cos\theta_{sur} + \sin\theta_{sur}) + \tau_{drag}\right\} \qquad (10)$$

where the shear stress $\tau_{drag}$ represents the drag force by the impinging plasma jet and $d\sigma/dT$ is the temperature gradient of the surface tension.

All heat transferred to the interface was assumed to be utilized either for melting

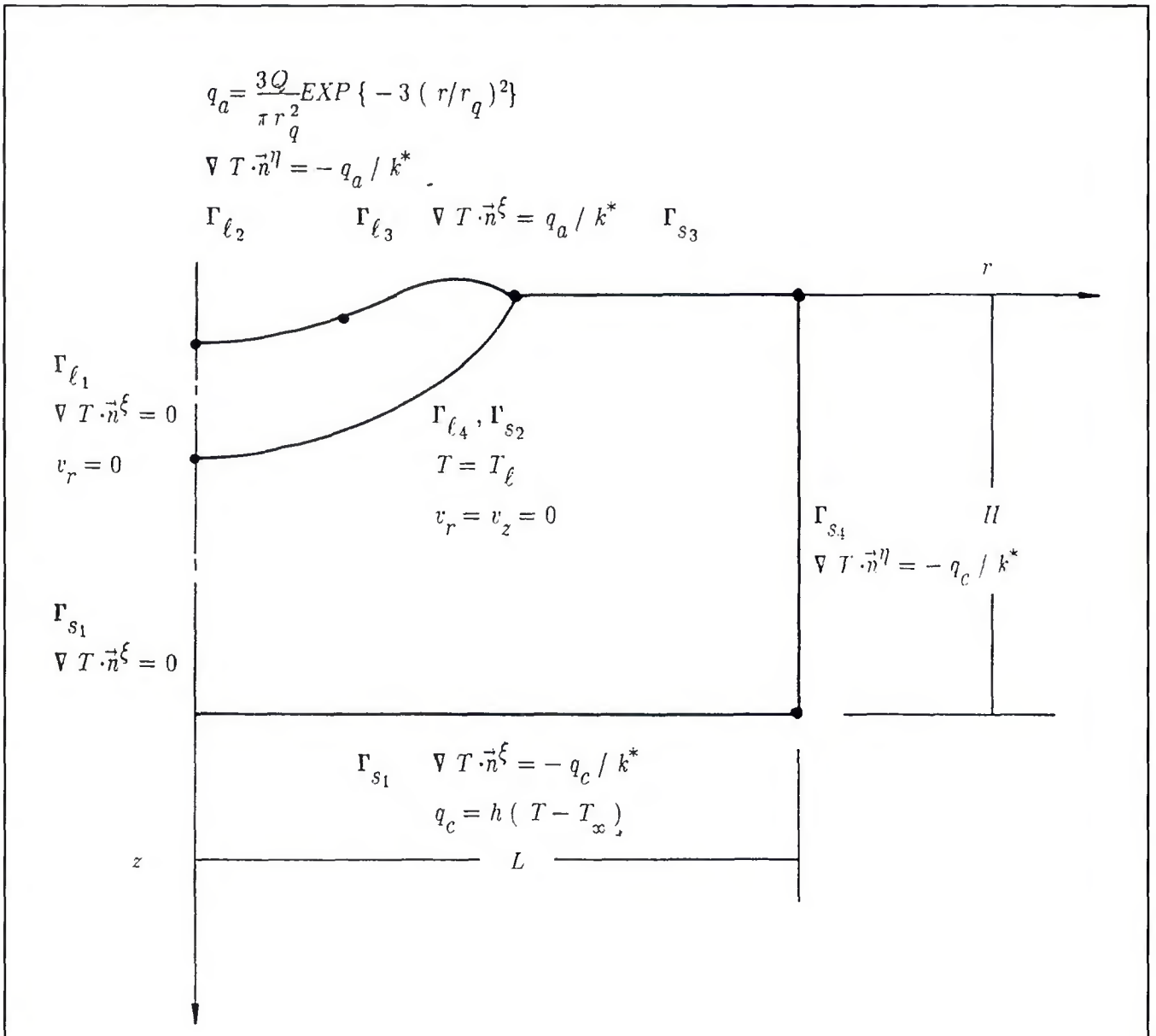


*Fig. 1—Boundary conditions for physical domain.*

or conduction to the solid, and therefore determines the propagation speed and the shape of the moving interface. This fact is stated by an energy balance at the melting interface, which is written as follows:

$$\rho h_f \frac{\partial n}{\partial t} = -k_\ell \frac{\partial T}{\partial n} + k_s \frac{\partial T}{\partial n} \qquad (11)$$

where n means the coordinate in the normal direction.

#### Surface Deformation

The weld pool surface under the arc pressure will form a shape that minimizes the total energy. Hence, it is convenient to use the equilibrium condition, by solving the variational problem subject to the constraint that the volume of the weld pool is constant. In the present study, it is assumed that the effect of weld pool convection on the weld surface deformation can be neglected. Thus, the total energy to be minimized includes the surface energy connected with the change in the area of the weld surface, the potential energy of the weld pool, and the work performed by the arc pressure displacing the weld pool surface. Accordingly the total energy is given by the following equation:

$$E_t = \int_0^r 2\pi r \left(\sigma\sqrt{1 + z_r^2} + \frac{1}{2}\rho g z^2 - p_{arc} z\right) dr \equiv \int_0^r F(r,z,z_r)\, dr \qquad (12)$$

where $z_r = dz/dr$ and $p_{arc}$ is the arc pressure.

Since the liquid metal volume in the weld pool is constant, the constraining equation is

$$\int_0^r 2\pi r z\, dr \equiv \int_0^r G(r,z)\, dr = \text{constant} \qquad (13)$$

The necessary condition for solution follows from the application of the appropriate Euler equation

$$\frac{\partial}{\partial r}\left\{\frac{\partial}{\partial z_r}(F + \lambda G)\right\} - \frac{\partial}{\partial z}(F + \lambda G) = 0 \qquad (14)$$

where λ is the Lagrangian multiplier. Substitution of the values previously defined into the Euler equation gives the following equation:

$$\sigma\left\{\frac{rz_{rr}+z_r(1+z_r^2)}{r(1+z_r^2)^{3/2}}\right\}=\rho gz-p_{arc}+\lambda \quad (15)$$

where the surface tension $\sigma$ at the weld pool surface was assumed to vary with the temperature as follows and the radial distribution of the arc pressure $p_{arc}$ employed was adopted from reference 11.[1]

$$\sigma(T)=\sigma(3000°C)+d\sigma/dT\,(T-3000) \quad (16)$$

where $\sigma(3000°C) = 1.1$ N/m (Ref. 11) In computational procedure, the iterative method of finite difference has been used to solve this nonlinear differential equation. After these calculations, the computational result is applied to the constraint prescribed. If it does not satisfy this constraint, the computation should be repeated after modification of λ in Equation 15.

## Numerical Procedure

### Transformation

To overcome the difficulties that arise due to the complex, time-dependent changing physical solution domain, a numerical transformation method was employed. The numerical transformation method employed is based on the automatic numerical generation of a general curvilinear coordinate system and was first developed and applied to fluid mechanical problems by Thompson, *et al.* (Ref. 12). The advantage of this transformation method is the fact that any set of equations of interest may be solved on a rectangular, uniformly spaced computational grid system which is fixed in space and time, as shown in Fig. 2. Therefore, this method is useful for the solution of moving boundary problems with a phase change such as GTA welding.

The boundary-fitted coordinates are obtained by the solution of the following system of quasi-linear elliptic partial differential equations with appropriate Dirichlet conditions along the boundaries.

$$\alpha r_{\xi\xi}-2\beta r_{\xi\eta}+\gamma r_{\eta\eta}+J^2(Rr_\xi+Sr_\eta)=0 \quad (17A)$$

$$\alpha z_{\xi\xi}-2\beta z_{\xi\eta}+\gamma z_{\eta\eta}+J^2(Rz_\xi+Sz_\eta)=0 \quad (17B)$$

where the coordinate control functions R and S may be chosen to influence the structure of the grid as desired. Figure 3 shows an example of the coordinate system created with this method.

### Transformation of Governing Equations and Boundary Conditions

To solve the given set of governing equations with the corresponding boundary conditions on the computational rectangular domain, all equations have to be transformed as in Appendix B.

### Numerical Scheme

To find the numerical solution of the transformed equations and boundary conditions, these equations were discretized using central difference approximations for all space derivatives. The standard finite difference technique adopted for the numerical solution of the energy equation and the vorticity equation was the alternating-direction implicit (ADI) scheme. The equation relating the stream function to vorticity was solved by the successive over-relaxation (SOR) method. Table 1

*1. Lin and Eagar calculated only the shape of the weld pool surface depression under the action of the arc pressure, based on the theory that the surface depression forms a shape which minimizes the total energy of the molten pool. In addition, for ease of analysis, they assumed that there is no convection in the molten pool.*

*But in this study, the authors intended to calculate not only the shape of the weld pool surface depression under the action of the arc pressure, but the shape of the liquid-solid interface formed from the convection heat transfer in the molten pool. In this convection heat transfer model, the driving forces to be considered are the buoyancy force, the electromagnetic force, the surface tension force, and the aerodynamic drag force. The purpose of this study was to calculate the weld pool geometry.*

*With respect to several other authors who have investigated the effect of weld pool surface deformation on weld penetration in gas tungsten arc welding, all of the previous researchers have used the rectangular coordinate system to solve the heat and fluid flow in the molten pool which has a deformed surface and irregular liquid-solid interface. In this study, a numerically generated boundary-fitted coordinate system was used to solve the transient melting problem.*

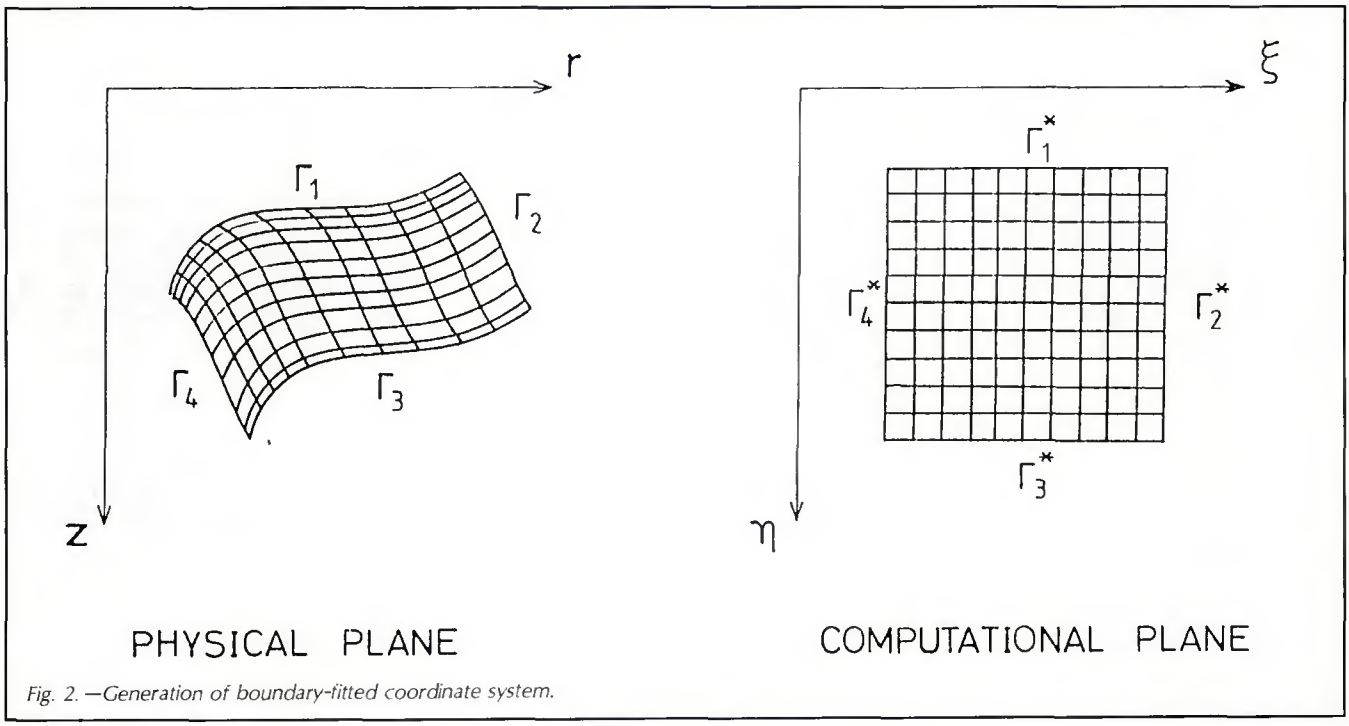


*Fig. 2.—Generation of boundary-fitted coordinate system.*

**Table 1—Parameters Used in the Computation**

| | |
|---|---|
| H = 5 mm | $T_\infty = 20°C$ |
| L = 10 mm | $T_\ell = 1530°C$ |
| $k_\ell = 15.48$ W/mK | $T_v = 3000°C$ |
| $c_\ell = 753$ J/kgK | $\mu = 0.006$ kg/m · s |
| $\rho = 7200$ kg/m$^3$ | $\mu_m = 0.26 \times 10^{-6}$ H/m |
| $\bar{\beta} = 10^{-4}$ 1/K | h = 10 W/mm$^2$°C |
| $d\sigma/dT = -10^{-5}$ N/m°C | $h_f = 247$ kJ/kg |

shows the parameters used in the calculation of the flow pattern. The temperature-dependent thermal conductivity and specific heat of AISI 1042 was used in the computation (Ref. 13). The radial distribution of the shear stress $\tau_{drag}$ employed has been adopted from reference (Ref. 14).

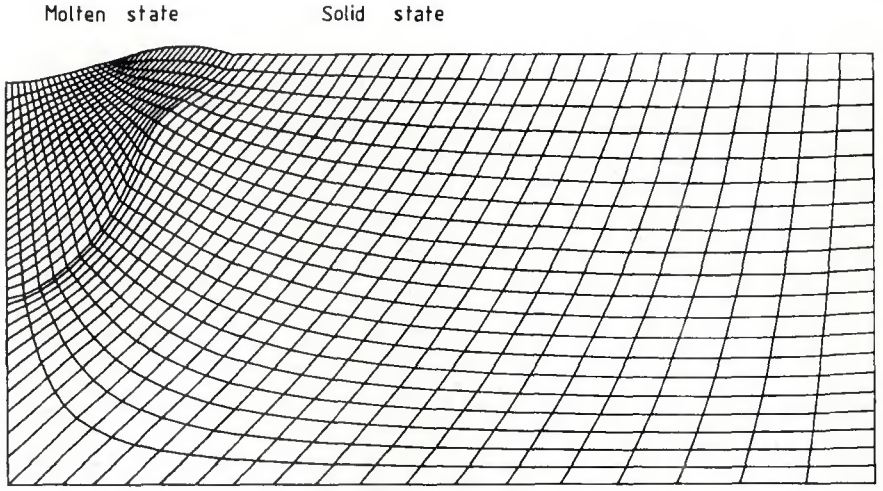

*Fig. 3—An example of grid generation.*

## Simulation Results and Discussion

The effect of the surface deformation on the weld penetration for I = 100 A is illustrated in Fig. 4 A–D, where the flow patterns and the fusion boundaries are plotted. By examining these results, it may be concluded that the shape of the flow pattern is little affected by the weld surface deformation. The reason for this behavior is that the maximum depth of the surface deformation is very small (calculated value: 0.02 mm) and that consequently it gives little effect on the weld pool convection.

Figure 5 shows the effect of the surface deformation on the weld penetration for I = 200 A in the case of pure conduction. As is to be expected, the result shows that the weld penetration is slightly larger in the case of the deformed surface than in the case of the flat surface. This phenomenon results from the fact that the heat transfer from the arc to the base metal becomes easier due to the arc pressure which depresses the molten pool surface, giving the heat flux access to a greater access in base metal.

Figure 6 A–D shows flow patterns that consider the convection driven by the buoyancy force, surface tension force and electromagnetic force. It can be seen that the velocity field consists of double-loop circulation patterns in the opposite direction—one at the weld pool surface and the other in the interior of the weld pool. The first loop is dominated by the surface tension force of the liquid metal, which is caused by the temperature gradient at the weld pool surface. Therefore, the flow driven by the surface tension should broaden the weld pool, while reducing the penetration in the central portion of the weld pool. The second one is dominated by the electromagnetic force, which is caused by the interaction between the divergent current path in the weld pool and the magnetic field it generates. The flow induced by the electromagnetic force allows the welding heat to be delivered quickly from the heat source to the weld root. Consequently, the transport of the hot liquid metal down along the axis of the weld pool will result in a deeper weld penetration. In other words, the electromagnetic force dominates at the axis of the weld pool and the surface tension force at the edge of the weld surface. Figure 6E, showing the shapes of the liquid-solid interface, reveals that in the effect of the convection on the weld penetration there is only a little difference between these two cases, and that the maximum surface depression at the center of the surface is deeper than that at I = 100 A.

In the same way, Fig. 7 A–E illustrates the effect of the weld surface deformation on the weld penetration and the flow pattern, for which the drag force is added to the driving force. The variation of the flow pattern calculated by considering the drag force on the weld pool surface is illustrated in Fig. 7 A–D. Figure 7 A and B are for a weld pool with the flat surface and Fig. 7 C and D for that with the deformed one. The flow patterns are very similar in two cases. The comparison of them with Fig. 6 A–D where the drag force is not considered shows that the flow at the edge of the weld pool surface is well developed, while that in the interior is rather weak. This is probably due to the effect of the drag force, which is not considered in Fig. 6 A–D. Although the surface tension force plays a role in the weld pool convection, the calculated weld penetration is dominated by the drag force. The reason for this behavior is that the temperature at the free surface is generally bounded by a limiting value (in this study, 3000°C/5432°F) corresponding to the temperature at which the heat loss by vaporization equals the incident heat flux. Near the center of the weld pool surface the temperature reaches this limiting value, and consequently, the effect of the surface tension force exists only at the edge of the weld pool surface, while the drag force works on the overall weld pool surface. Such a phenomenon is more evident in Fig. 7 C and D with the deformed surface than in Fig. 7 A and B with the flat surface. It can be seen in Fig. 7 C and D that the flow on the weld pool surface is extended up to the central area, and that the flow in the interior of the weld pool by the electromagnetic force becomes weaker than in Fig. 6 C and D. In addition, these flow patterns affect the weld pool shape directly. From the comparison of Fig. 7 E with Fig. 6 E, it can be seen that the weaker flow in the interior of the weld pool reduces the penetration, while the stronger flow at the edge broadens its width.

For these flow patterns, the variation of the liquid-solid interface is shown in Fig. 7 E. There is a reverse trend against the previous cases (Figs. 5 and 6), where the weld penetration with the deformed weld surface is deeper than that with the flat weld surface. Although in the deformed weld surface the conductive heat transfer path from the weld pool surface to the liquid-solid interface is short, the radially outward flow pattern strengthened by the drag force reduces the heat transfer from the arc to the weld interface, thus producing a shallow weld penetration.

In a similar method, Fig. 8, Fig. 9 A–D and Fig. 10 A–E reveal that the differences in the weld penetration and the flow patterns are more evident for I = 300 A than for I = 200 A. In the case of pure conduction for I = 300 A, the weld pool shape becomes deeper and wider than for I = 200 A—Fig. 8. In Fig. 9 A–D where the flow patterns are illustrated without the

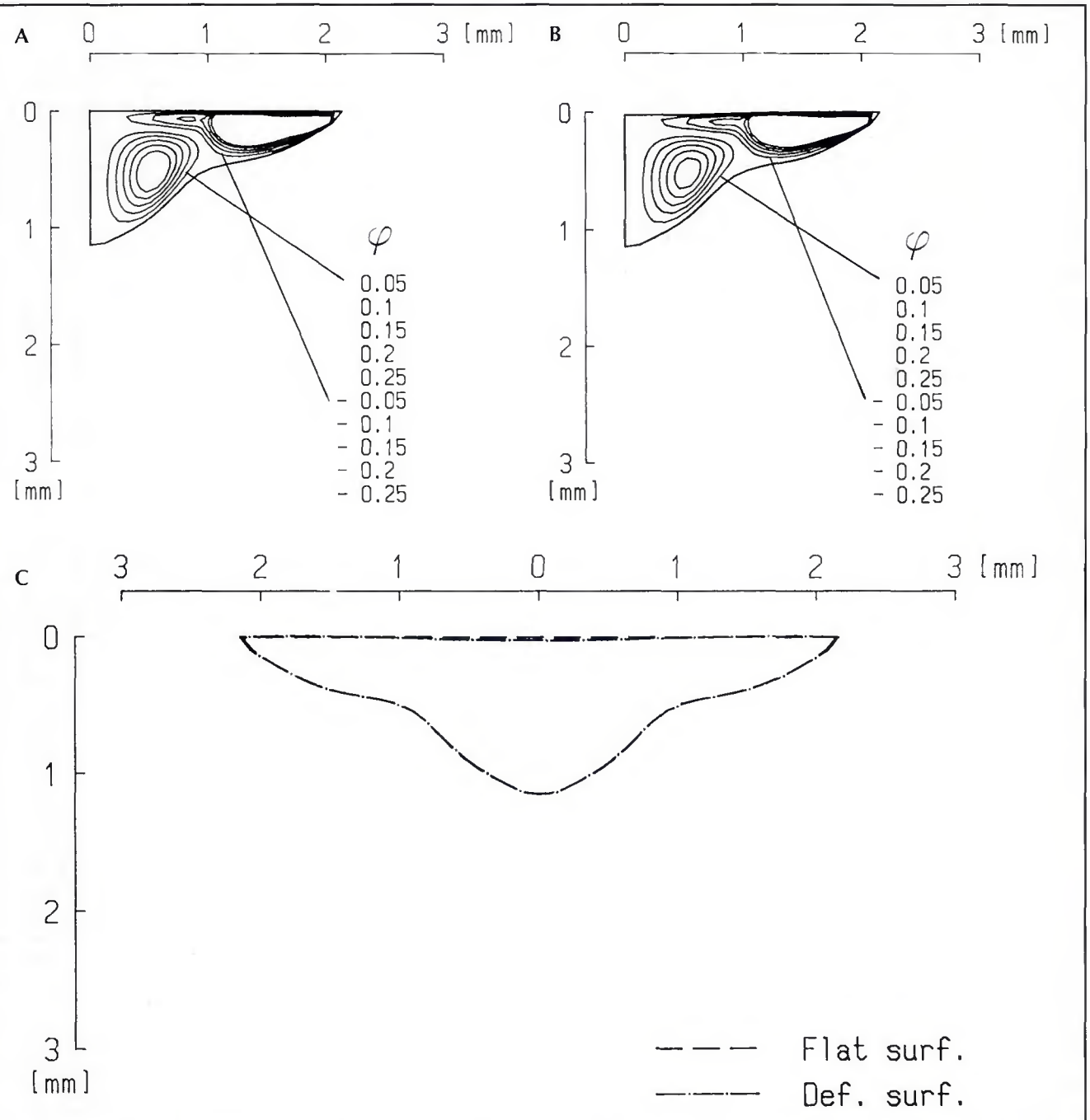


*Fig. 4.—Flow pattern and fusion boundaries in flat and deformed surface for I = 100 A after 1 s welding. A—Stream line contours of various stream functions for flat surface; B—stream line contours of various stream functions for deformed surface; C—Comparison of fusion boundaries.*

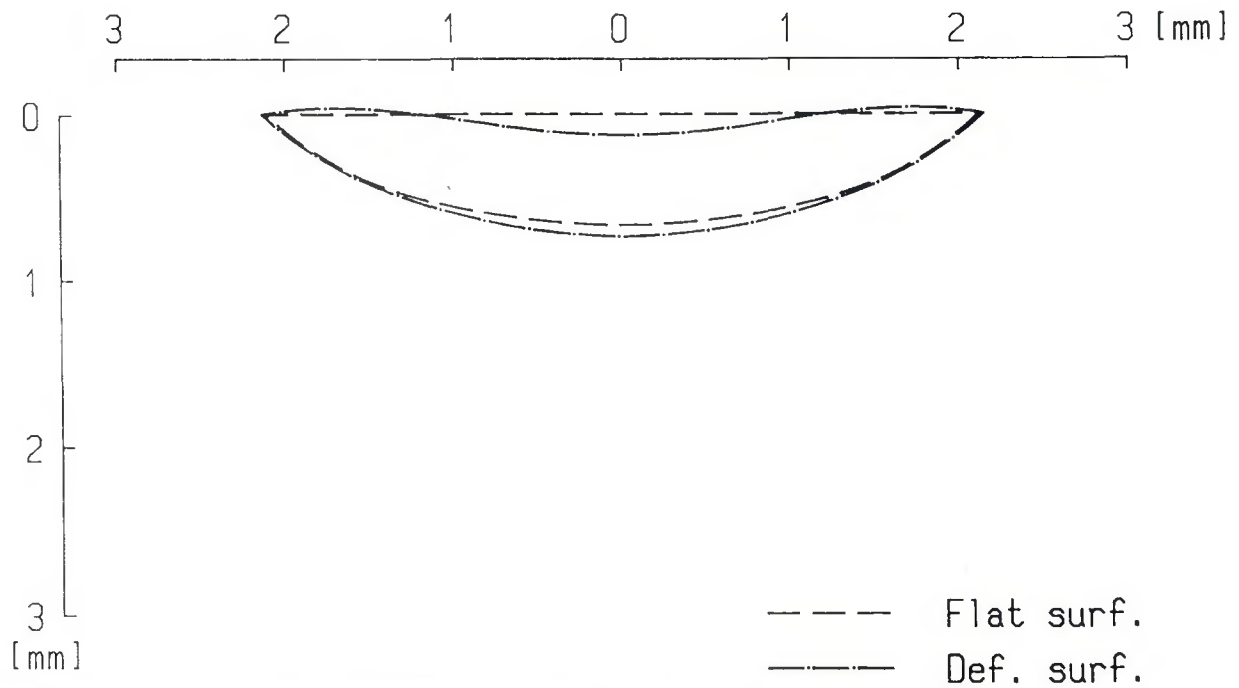


*Fig. 5.—Comparison of fusion boundaries for pure conduction for I = 200 A after 1 s of welding.*

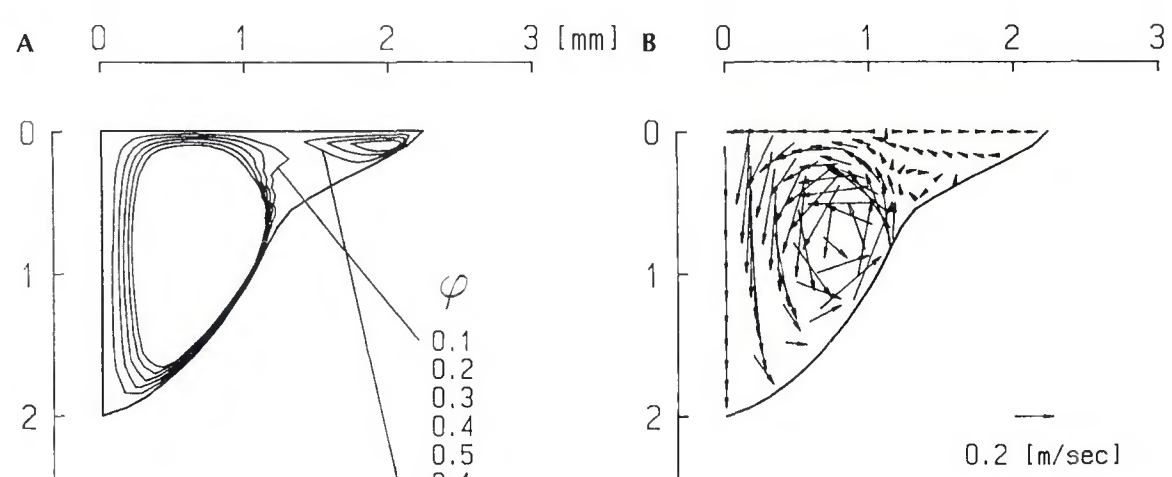


*Fig. 6—Flow patterns due to buoyancy force, electromagnetic force and surface tension force for I = 200 A after 1 s of welding. A—Stream line contours of various stream functions for flat surface; B—velocity distribution for flat surface; C (next page)—stream line contours of various stream functions for deformed surface; D—velocity distribution for deformed surface; E—Comparison of fusion boundaries for flat and deformed surface.*

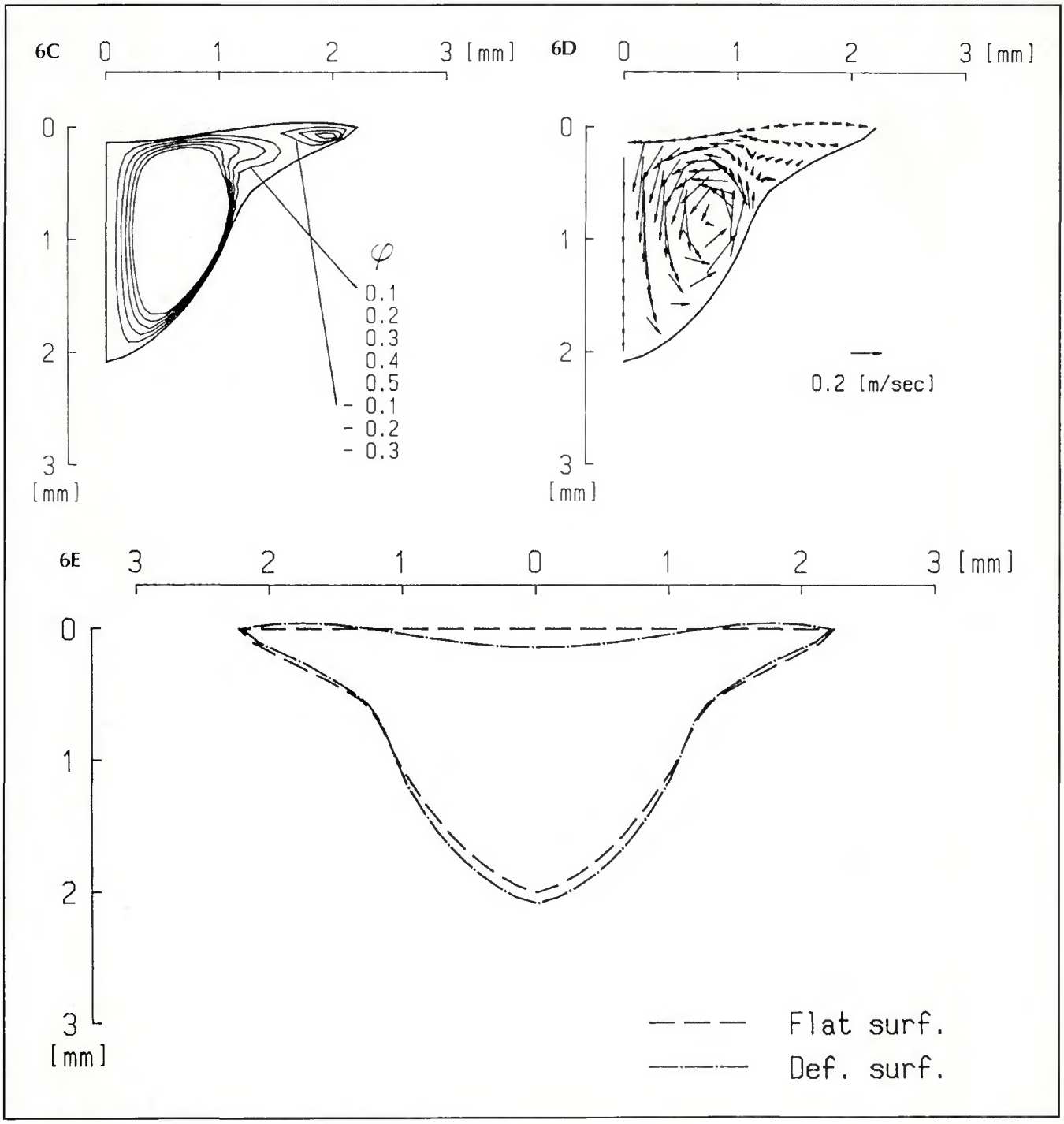
6C
0
1
2
3 [mm]
0
1
2
3
[mm]
φ
0.1
0.2
0.3
0.4
0.5
- 0.1
- 0.2
- 0.3
6D
0
1
2
3 [mm]
0
1
2
3
[mm]
0.2 [m/sec]
6E
3
2
1
0
1
2
3 [mm]
0
1
2
3
[mm]
Flat surf.
Def. surf.

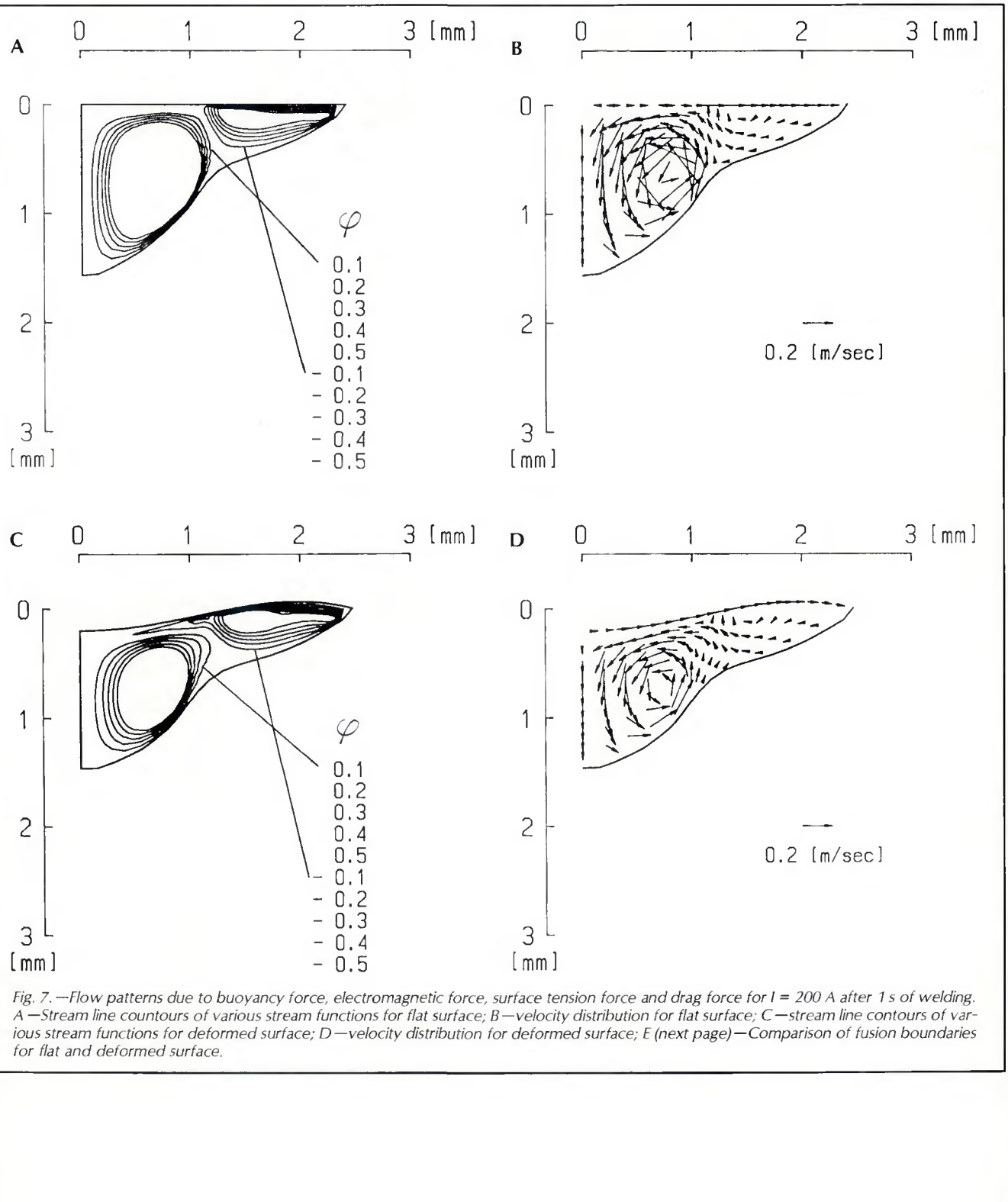


*Fig. 7.—Flow patterns due to buoyancy force, electromagnetic force, surface tension force and drag force for I = 200 A after 1 s of welding. A—Stream line countours of various stream functions for flat surface; B—velocity distribution for flat surface; C—stream line contours of various stream functions for deformed surface; D—velocity distribution for deformed surface; E (next page)—Comparison of fusion boundaries for flat and deformed surface.*

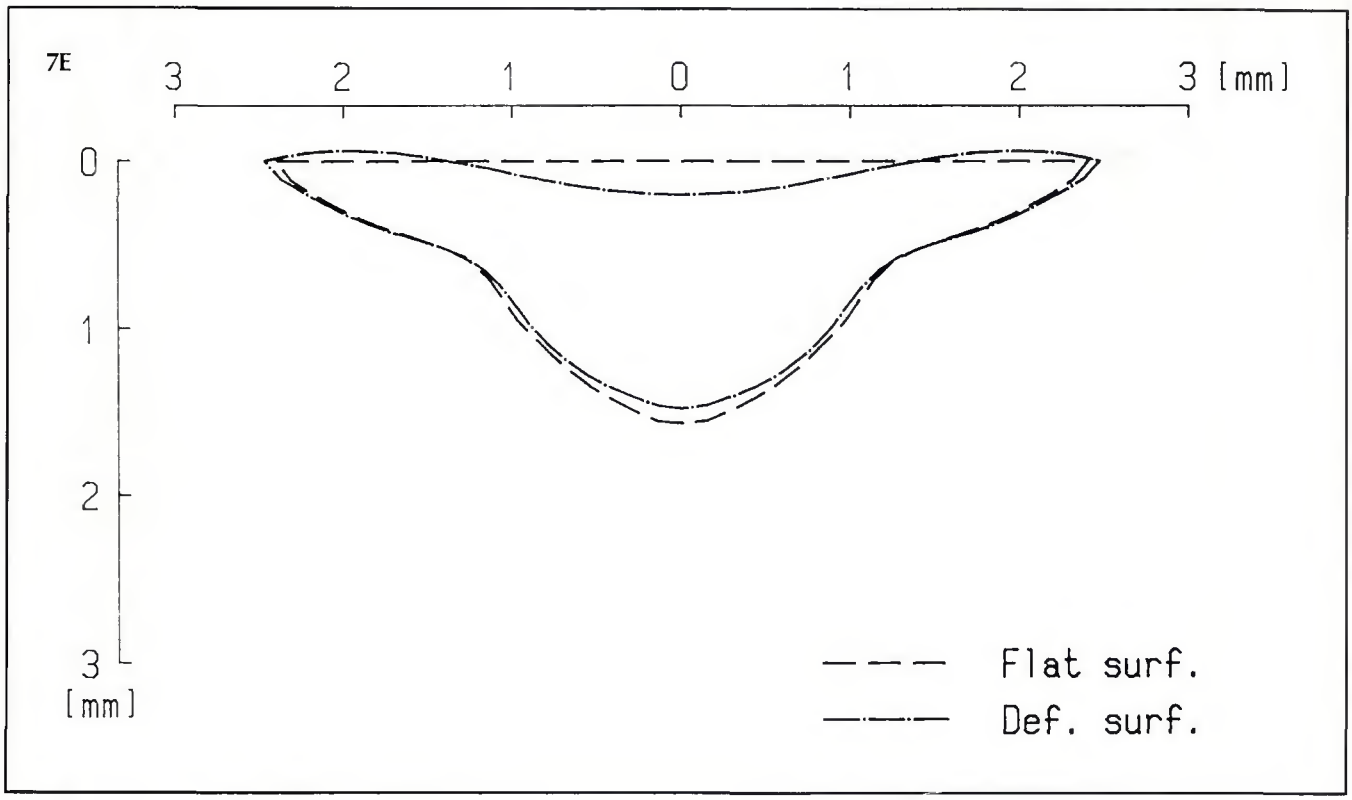


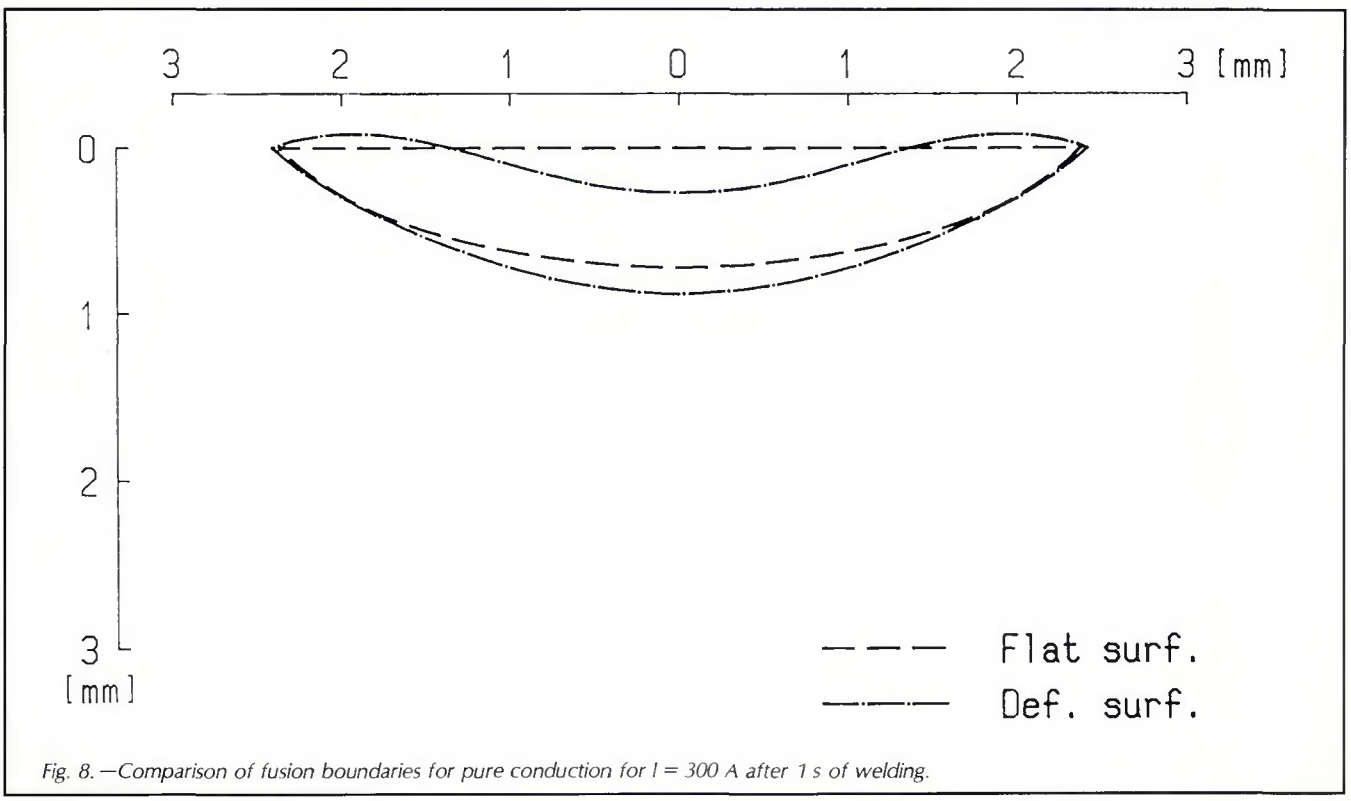


*Fig. 8.—Comparison of fusion boundaries for pure conduction for I = 300 A after 1 s of welding.*

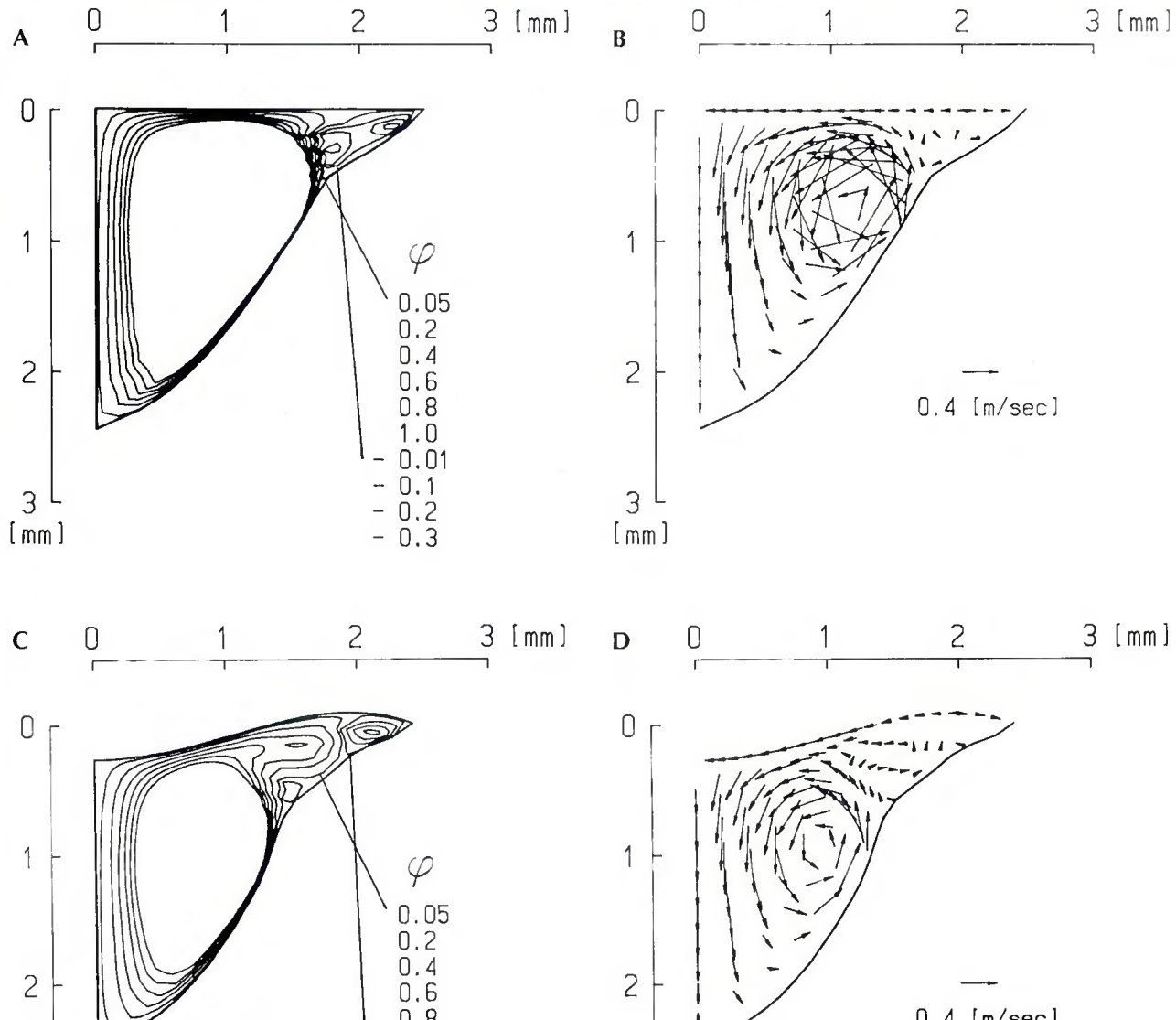


*Fig. 9—Flow patterns due to buoyancy force, electromagnetic force and surface tension for I = 300 A after 1 s of welding. A—Stream line contours of various stream functions for flat surface; B—velocity distribution for flat surface; C—stream line contours of various stream functions for deformed surface; D—velocity distribution for deformed surface; E (next page)—comparison of fusion boundaries for flat and deformed surface.*

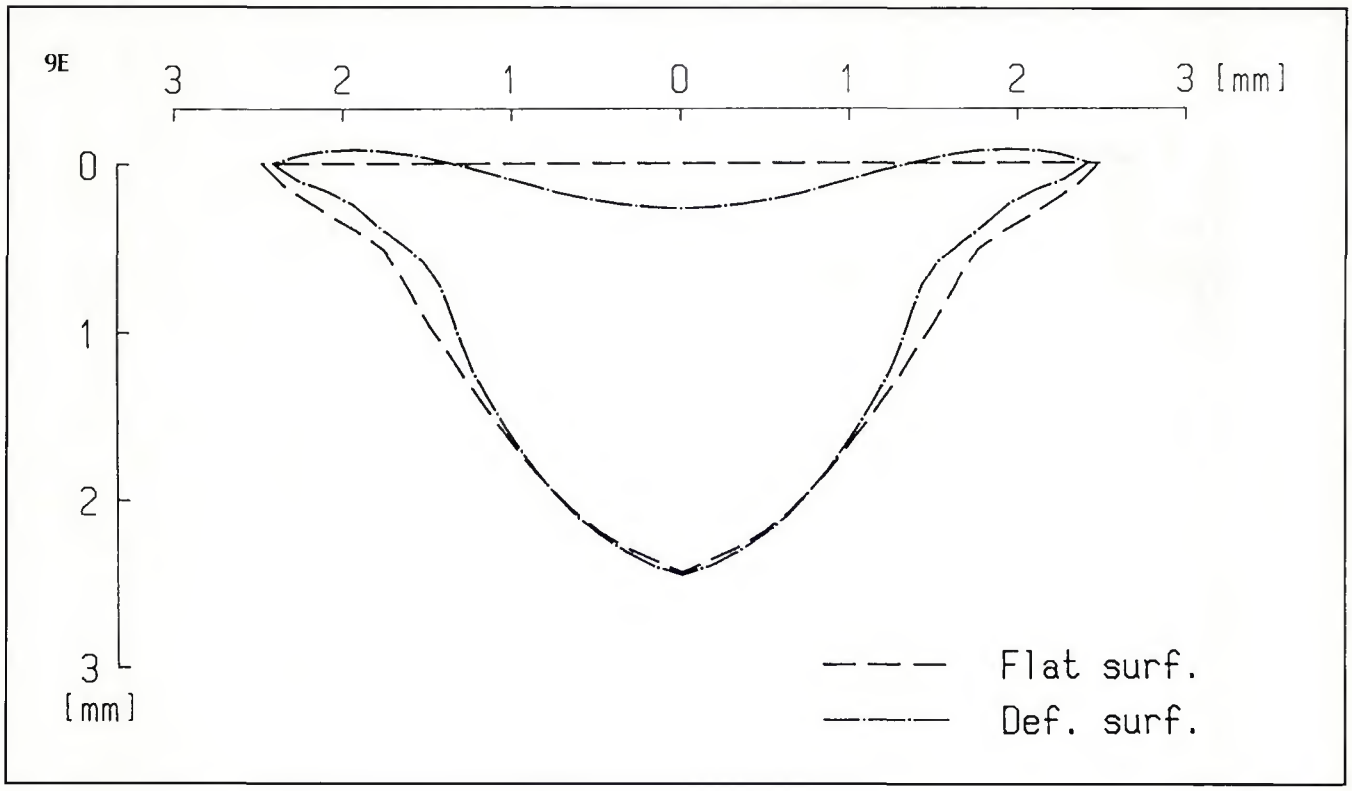


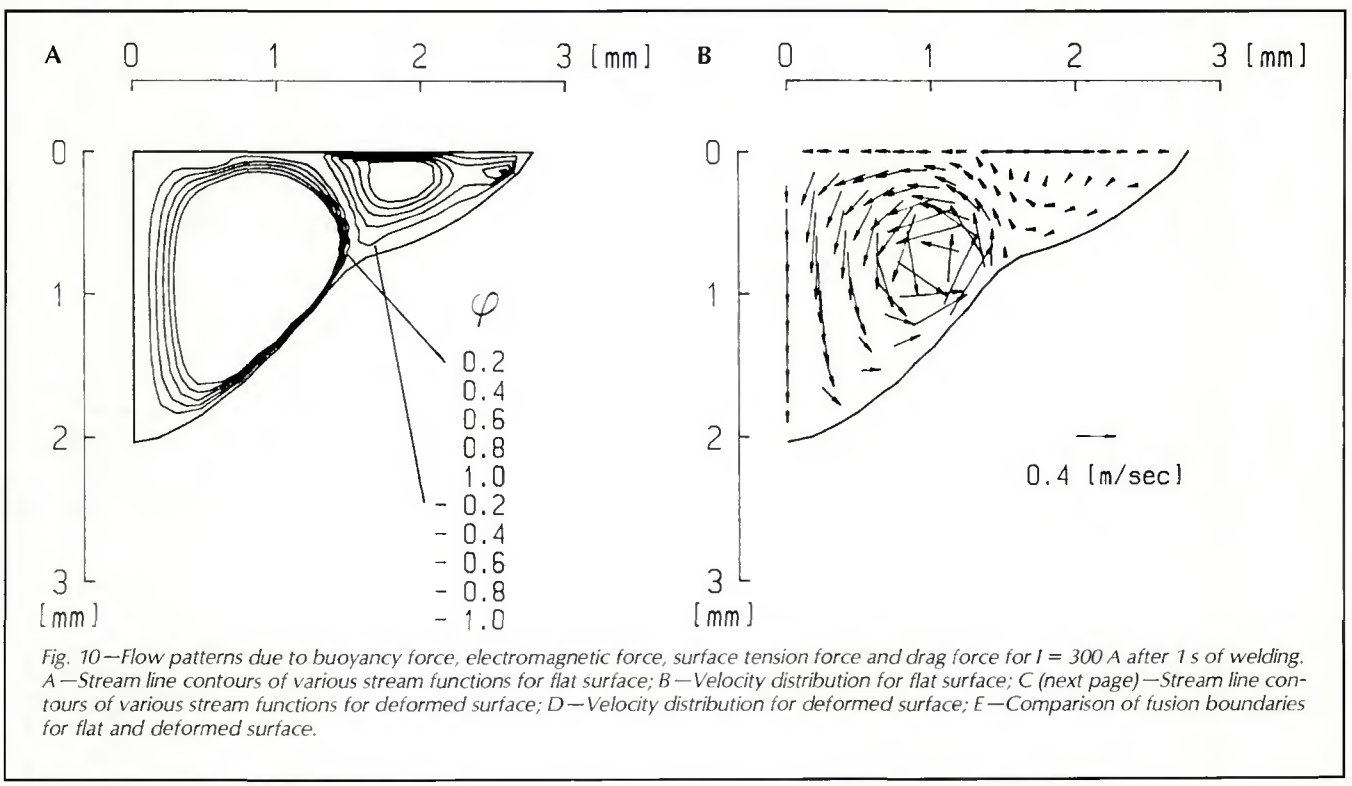


*Fig. 10—Flow patterns due to buoyancy force, electromagnetic force, surface tension force and drag force for I = 300 A after 1 s of welding. A—Stream line contours of various stream functions for flat surface; B—Velocity distribution for flat surface; C (next page)—Stream line contours of various stream functions for deformed surface; D—Velocity distribution for deformed surface; E—Comparison of fusion boundaries for flat and deformed surface.*

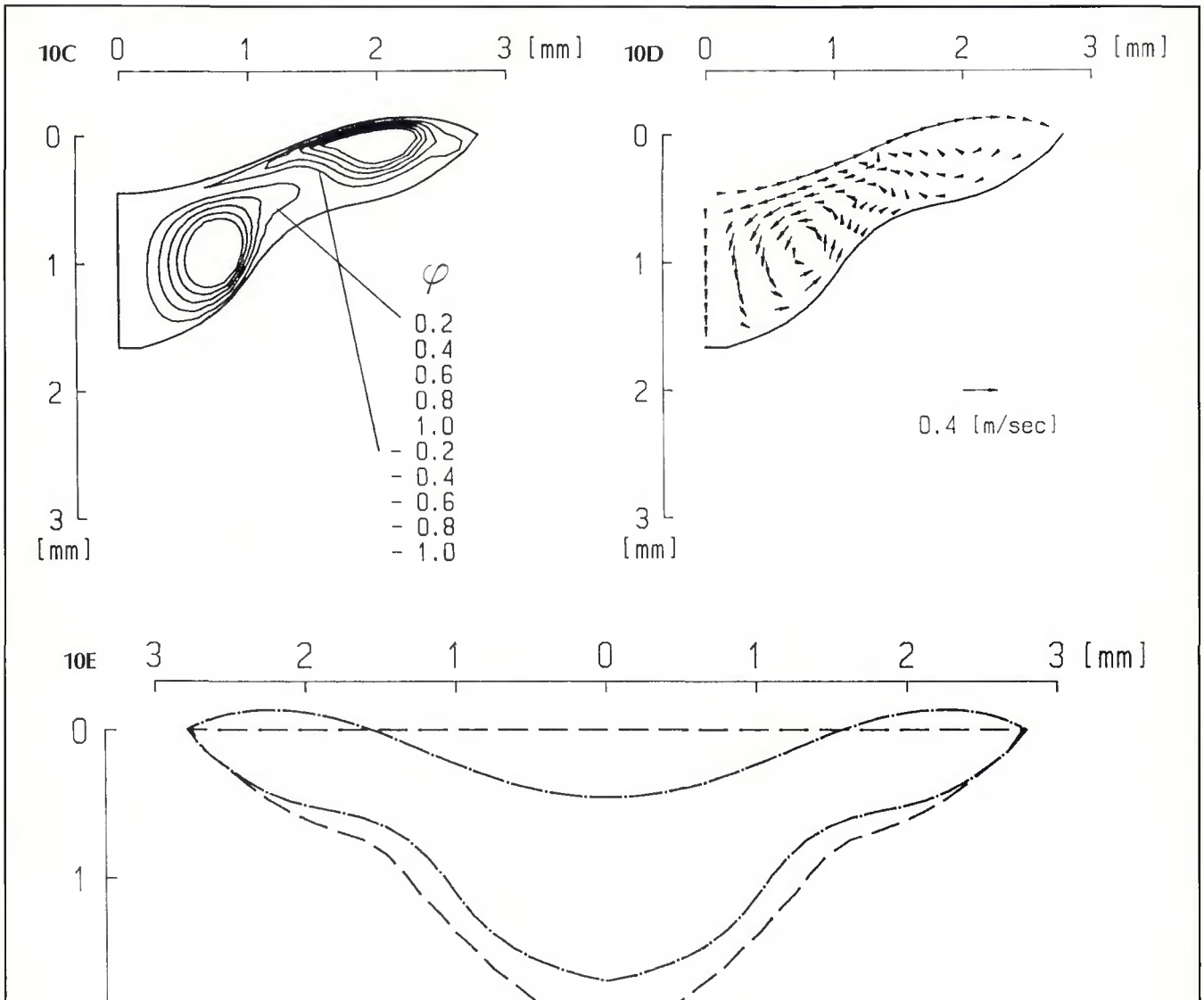
10C
0 1 2 3 [mm]
0
1
2
3
[mm]
φ
0.2
0.4
0.6
0.8
1.0
- 0.2
- 0.4
- 0.6
- 0.8
- 1.0
10D
0 1 2 3 [mm]
0
1
2
3
[mm]
0.4 [m/sec]
10E
3 2 1 0 1 2 3 [mm]
0
1
2
3
[mm]
Flat surf.
Def. surf.

drag force, it can be seen that there is little difference between the two flow patterns, which results in little difference of the weld penetration. On the other hand, Fig. 10 A-D shows the very different flow patterns with the drag force, especially in the interior of the weld pool. As a result, it can be seen that the difference in weld penetration between Fig. 10E and Fig. 9E is larger than that between Fig. 6E and Fig. 7E. Accordingly, it can be concluded that the more the current increases, the stronger the effect of the drag force on the flow pattern is, which results in a larger difference in the weld pool shape. In addition, it is apparent, as discussed earlier, that for the deformed weld surface the velocity of the molten metal decreases markedly, which is explained as follows: As the weld surface deformation increases to large values, the drag force becomes dominant in the weld pool convection, thus impeding the flow induced by the electromagnetic force.

## Summary and Conclusions

The transient axisymmetric weld pool convection problem in GTA welding was simulated by a numerical model. In computer modeling, a number of previous researchers have considered only three forces as driving forces for weld pool convection, neglecting the drag force. In this study, the four distinct driving forces were considered—the buoyancy force, electromagnetic force, drag force, and surface tension force on the weld pool surface.

As the solution methodology, a numerically generated boundary-fitted coordinate system was used to solve the transient melting problem, which is generally known as the moving boundary problem. This method was useful for the implementation of the latent heat effect and for the formulation of the boundary conditions at the arbitrarily shaped liquid-solid interface and the weld pool surface deformed by the arc pressure.

For the welding current of 100 A, the shape of liquid-solid interface is little affected by the weld surface deformation. This is due to the fact that the maximum depth of the surface deformation is very small and that consequently it gives only a little effect on the weld pool convection.

If the weld pool surface is deformed by the welding current of 200 and 300 A, it encourages the conductive heat transfer from the arc to the liquid-solid interface. But in the case of excessive deformation, the velocity of flow in the weld pool markedly decreases. As the weld surface deformation becomes very large, the drag force becomes dominant in the weld pool convection, thus impeding the flow induced by the electromagnetic force, and producing a shallow weld penetration. This is attributed to the fact that the drag force, which works on the weld pool surface, is assumed to increase in proportion to the increase of weld pool surface area. In the flow patterns calculated with the flat and the deformed surface for I = 300 A, these differences are more evident than for I = 200 A.

*Acknowledgment*

The authors gratefully acknowledge the support from the Ministry of Science and Technology, Republic of Korea.

*References*

1. Shaw, C. B., Jr. 1975. Diagonostic studies of the GTAW arc. *Welding Journal* 54(3):81-s to 86-s.

2. Friedman, E. 1978. Analysis of weld puddle distortion and its effect on penetration. *Welding Journal* 57(6):161-s to 166-s.

3. Oper, G. M., and Szekely, J. 1984. Heat and fluid flow phenomena in weld pools. *J. of Fluid Mechanics*, Vol. 147, pp. 53-79.

4. Kou, S., and Wang, Y. H. 1986. Computer simulation of convection in moving arc weld pools. *Metall. Trans.*, Vol. 17A, No. 12, pp. 2271-2277.

5. Wilson, D. G., Solomon A. D., and Boggs, P. T. 1978. *Moving Boundary Problems*. Academic Press, U.K.

6. Rao, P. R., and Sastri, V. M. K. 1984. Efficient numerical method for two-dimensional phase change problems. *Int. J. of Heat and Mass Transfer*, Vol. 27, No. 11, pp. 2077-2084.

7. Bain, R. L., Stermole, F. J., and Golden, J. O. 1974. Liquefaction dynamics of n-octadecane in cylindrical coordinates. *J. of Spacecraft*, Vol. 11, No. 5, pp. 335-339.

8. Hong, C. P., Umeda, T., and Kimura, Y. 1984. Numerical models for casting solidification: part II. application of the boundary element method to solidification problems. *Metall. Trans.*, Vol. 158, No. 3, pp. 101-107.

9. Rieger, H., Projahn, U., and Beer, H. 1982. Analysis of the heat transport mechanisms during melting around a horizontal circular cylinder. *Int. J. of Heat and Mass Transfer*, Vol. 25, No. 1, pp. 137-147.

10. Kim, S.-D., and Na, S.-J. 1989. A study on heat and mass flow in stationary gas tungsten arc welding using the numerical mapping method. *Proc. Inst. Mech. Eng. Part B: J. of Engineering Manufacture*, Vol. 203, pp. 233-242.

11. Lin, M. L., and Eagar, T. W. 1985. Influence of arc pressure on weld pool geometry. *Welding Journal* 64(6):163-s to 169-s.

12. Thompson, J. F., Thames, F. C., and Mastin, C. W. 1974. Automatic numerical generation of body-fitted curvilinear coordinate system containing any number of arbitrary two-dimensional bodies. *J. of Comp. Phys.*, Vol. 15, No. 1, pp. 299-319.

13. *Metals Handbook*, Ninth edition, ASM International, 1978, Vol. 1, pp. 145-151.

14. Matsunawa, A., Yokoya, S., and Asako, Y. 1988. Convection in weld pool and its effect on penetration shape in stationary arc welds. *J. of Japan Welding Soc., Vol. 6, No. 4, pp. 455-462.*

## Appendix A: Nomenclature

| | |
|---|---|
| B | magnetic flux vector |
| $B_\theta$ | $\theta$-component of magnetic flux vector B |
| c | specific heat |
| $c_\ell$, $c_s$ | specific heat of molten and solid |
| $E_t$ | total energy |
| F | body force vector |
| $F_r$, $F_z$ | r- and z-component of body force vector F |
| Fo | Fourier number |
| g | gravitational acceleration |
| h | heat transfer coefficient |
| H, L | depth and width of solution domain |
| $h_f$ | latent heat of fusion |
| I | welding current |
| J | Jacobian of transformation |
| J | Current density vector |
| $J_r$, $J_z$ | r- and z-component of current density vector J |
| k | thermal conductivity |
| $k_\ell$, $k_s$ | thermal conductivity of molten and solid |
| $\ell_{arc}$ | arc length |
| $\ell$ | length along the weld pool surface |
| n | coordinate in normal direction |
| $\vec{n}_\xi$, $\vec{n}_\eta$ | unit normal vector to a line of constant $\xi$ and $\eta$ |
| $p_{arc}$ | arc pressure |
| Pr | Prandtl number |
| Q | total heat input |
| $q_a$ | heat density distribution of arc $q_a = \frac{3Q}{\pi r_q^2} \text{EXP}\left\{-3\left(\frac{r}{r_q}\right)^2\right\}$ |
| $q_c$ | heat loss by free convection $q_c = h\,(T - T_\infty)$ |
| r, z | radial and axial direction of cylindrical coordinate system |
| R, S | coordinate control function |
| $r_q$, $r_i$ | effective radius of heat and current flux |
| Ste | Stefan number |
| $T_\ell$, $T_s$ | liquidus and solidus temperature |
| $T_v$ | maximum temperature of weld pool surface |
| $T_\infty$ | ambient temperature |
| V | velocity vector |
| $v_r$, $v_z$ | r- and z-component of velocity vector V |

**Greek Symbols**

| | |
|---|---|
| $\alpha$, $\beta$, $\gamma$ | transformation factors $\alpha = r_\eta^2 + z_\eta^2, \beta = r_\xi r_\eta + z_\xi z_\eta, \gamma = r_\xi^2 + z_\xi^2$ |
| $\bar{\alpha}$ | thermal diffusivity |
| $\alpha_\ell$, $\alpha_s$ | thermal diffusivity of molten and solid state |
| $\bar{\beta}$ | thermal expansion coefficient |
| $\Gamma$ | boundary |
| $\theta$ | dimensionless temperature |
| $\theta_{sur}$ | angle between r-axis and the tangential line along the weld pool surface where, the angle from r-axis toward z-axis is positive |
| $\xi$, $\eta$ | coordinate direction in transformed plane |
| $\rho$ | density |
| $\sigma$ | surface tension |
| $d\sigma/dT$ | temperature gradient of surface tension |
| $\tau$ | dimensionless time |
| $\tau_{drag}$ | shear stress |
| $\psi$ | stream function |
| $\mu$ | viscosity |
| $\mu_m$ | magnetic permeability |

$\omega$ vorticity
$\lambda$ Lagrangian multiplier

$$\frac{D}{Dt} \equiv \frac{\partial}{\partial t} + v_r \frac{\partial}{\partial z} + v_z \frac{\partial}{\partial z}$$

$$\nabla^2 \equiv \frac{\partial^2}{\partial r^2} + \frac{1}{r}\frac{\partial}{\partial r} + \frac{\partial^2}{\partial z^2}$$

**Subscripts**

$\ell$ molten state
s solid state
$\xi, \eta, \tau$ derivative with respect to $\xi, \eta, \tau$
r, z, $\theta$ r-, z-, $\theta$-component

## Appendix B: Transformation of Equations

Before the transformation, the governing equation and boundary condition were brought into nondimensional form by defining the following dimensionless variables:

$$r^* = \frac{r}{L},\ z^* = \frac{z}{L},\ \theta = \frac{T - T_\ell}{T_v - T_\ell}$$

$$\tau = \left(\frac{\bar{\alpha}_\ell t}{L^2}\right) \cdot \left(\frac{c_\ell (T_v - T_\ell)}{h_f}\right) = Fo \cdot Ste \tag{A1}$$

$$\omega^* = \frac{\omega}{\bar{\alpha}_\ell / L^2},\ \psi^* = \frac{\psi}{\bar{\alpha}_\ell L}$$

$$Pr = \frac{\nu}{\bar{\alpha}_\ell},\ Ra = \frac{\bar{\beta} g L^3 (T_v - T_\ell)}{\bar{\alpha}_\ell \nu}$$

Use of these transformations converts the governing equations and the corresponding boundary conditions to the following form:

Governing equations

$$Ste \cdot J \cdot \omega_\tau + \left\{\left(-\frac{\psi_\eta}{\eta} - Pr\frac{z_\eta}{r}\right)\omega - Pr\frac{\alpha}{J}\omega_\xi\right\}\xi + \left\{\left(\frac{\psi_\xi}{r} + Pr\frac{z_\xi}{r}\right)\omega - Pr\frac{\gamma}{J}\omega_\eta\right\}_\eta$$
$$= Pr\left\{-\left(\frac{\beta}{J}\omega_\eta\right)_\xi - \left(\frac{\beta}{J}\omega_\xi\right)\eta\right\} + Pr \cdot R\alpha\left\{(z_\eta\theta)_\xi - (z_\xi\theta)_\eta\right\}$$
$$-\left(\frac{L}{\rho\bar{\alpha}_\ell^2}\right)\left\{(r_\xi B_\theta J_z)_\eta - (r_\eta B_\theta J_z)_\xi + (z_\eta B_\theta J_r)_\xi - (z_\xi B_\theta J_r)_\eta\right\} \tag{A2}$$

$$\left(\frac{z_\eta}{r}\psi - \frac{\alpha}{J}\psi_\xi\right)_\xi + \left(-\frac{z_\xi}{r}\psi - \frac{\gamma}{J}\psi_\eta\right)_\eta = -\left(\frac{\beta}{J}\psi_\xi\right)_\xi - \left(\frac{\beta}{J}\psi_\xi\right)_\eta + J \cdot r \cdot \omega \tag{A3}$$

$$SteJ\theta_\tau + \left\{\left(-\frac{\psi_\eta}{r} - \bar{\alpha}^*\frac{z_\eta}{r}\right)\theta - \bar{a}^*\frac{\alpha}{J}\theta_\xi\right\}\xi + \left\{\left(\frac{\psi_\xi}{r} + \bar{\alpha}^*\frac{z_\xi}{r}\right)\theta - \bar{\alpha}^*\frac{\gamma}{J}\theta_\eta\right\}_\eta$$
$$= \bar{\alpha}^*\left\{-\left(\frac{\beta}{J}\theta_\eta\right)_\xi - \left(\frac{\beta}{J}\theta_\xi\right)_\eta\right\} + \frac{\theta}{r^2}\left\{(r_\xi\psi)_\eta - (r_\eta\psi)_\xi\right\} \tag{A4}$$

where $\bar{\alpha}^* = \bar{\alpha}/\bar{\alpha}_\ell$ $\begin{cases}\bar{\alpha}^* = 1 & \text{in molten state}\\ \bar{\alpha}^* = \bar{\alpha}_s/\bar{\alpha}_\ell & \text{in solid state}\end{cases}$

and the asterisks have been omitted from scaled variables.

Boundary Conditions

$\Gamma_{l1}$ $\omega = 0, \psi = 0$

$\alpha\,\theta_\xi - \beta\,\theta_\eta = 0$

$\Gamma_{l2}$ $\omega = -\dfrac{L^2}{\mu\bar{\alpha}_\ell}\left\{\left(\dfrac{\Delta T}{L}\right)\left(\dfrac{d\sigma}{dT}\right)\left(\dfrac{\theta_\xi}{\ell_\xi}\right)(\cos\theta_{sur} + \sin\theta_{sur}) + \tau_{drag}\right\}, \psi = 0$

$\gamma\,\theta_\eta - \beta\,\theta_\xi = -J\sqrt{\gamma}\dfrac{q_a L}{k^*\,\Delta T}$

$\Gamma_{\ell 3}$ $\omega = -\dfrac{L^2}{\mu\bar{\alpha}_\ell}\left\{\left(\dfrac{\Delta T}{L}\right)\left(\dfrac{d\sigma}{dT}\right)\left(\dfrac{\theta_\eta}{\ell_\eta}\right)(\cos\theta_{sur} + \sin\theta_{sur}) + \tau_{drag}\right\}, \psi = 0$

$\alpha\,\theta_\xi - \beta\,\theta_\eta = J\sqrt{\alpha}\dfrac{q_a L}{k^*\Delta T}$

$\Gamma_{\ell 4}$ $\omega = -\dfrac{\gamma}{rJ^2}\psi_{\eta\eta}$, $\psi = 0$ (A5)

$\theta = 1.$

$\Gamma_{s1}$ $\begin{cases}\alpha\,\theta_\xi - \beta\,\theta_\eta = 0 & (r = 0)\\ \alpha\,\theta_\xi - \beta\,\theta_\eta = -J\sqrt{\alpha}\ \dfrac{q_c L}{k^*\,\Delta T} & (r \neq 0)\end{cases}$

$\Gamma_{s2}$ $\theta = 1.$

$\Gamma_{s3}$ $\alpha\,\theta_\xi - \beta\,\theta_\eta = J\sqrt{\alpha}\dfrac{q_a L}{k^*\,\Delta T}$

$\Gamma_{s4}$ $\gamma\,\theta_\eta - \beta\,\theta_\xi = -J\sqrt{\gamma}\dfrac{q_c L}{k^*\,\Delta T}$

$$r_\tau = -\left(\frac{k_s}{k_\ell}\right)\left(\frac{z_\xi\theta_\eta}{J}\right)_s + \left(\frac{z_\xi\theta_\eta}{J}\right)_\ell \tag{A6}$$

$$z_\tau = \left(\frac{k_s}{k_\ell}\right)\left(\frac{r_\xi\theta_\eta}{J}\right)_s - \left(\frac{r_\xi\theta_\eta}{J}\right)_\ell \tag{A7}$$

# WRC Bulletin 364
# June 1991

This bulletin contains two reports:

## (1) New Design Curves for Torispherical Heads

**By A. Kalnins and D. P. Updike**

## (2) Elastic-Plastic Analysis of Shells of Revolution under Axisymmetric Loading

**By D. P. Updike and A. Kalnins**

Publication of these reports was sponsored by the Committee on Shells and Ligaments of the Pressure Vessel Research Council. The price of WRC Bulletin 364 is $40.00 per copy, plus $5.00 for U.S. and $10.00 for overseas, postage and handling. Orders should be sent with payment to the Welding Research Council, Room 1301, 345 E. 47th St., New York, NY 10017.

---

# WRC Bulletin 369
# December 1991

## Nitrogen in Arc Welding — A Review

**By IIW Commission II**

In 1983, Commission II of the International Institute of Welding (IIW) initiated an effort to review and examine the role of nitrogen in steel weld metals. The objective was to compile in one source, for future reference, the available information on how nitrogen enters weld metals produced by various arc welding processes, what forms it takes in these welds, and how it affects weld metal properties.

This bulletin contains 13 reports and several hundred references related to Nitrogen in Weld Metals that has been prepared as a review to show the importance nitrogen has in determining weld metal properties.

Publication of this report was sponsored by the Welding Research Council, Inc. The price of WRC Bulletin 369 is $85.00 per copy, plus $5.00 for U.S. and $10.00 for overseas, postage and handling. Orders should be sent with payment to the Welding Research Council, Room 1301, 345 E. 47th St., New York, NY 10017.